Humidity resistant carbon nanotubes-styrene methyl-methacrylate polymer composite for ultrafast laser

*Yunliang Bao [1]†, Lilong Dai [1]†, Junjie Jiang [1], Zinan Huang [1], Qianqian Huang [1] , Aleksey Rozhin[2] and Chengbo Mou [1]**

[1]Key Laboratory of Specialty Fiber Optics and Optical Access Networks, Shanghai Institute for Advanced Communication and Data Science, Joint International Research Laboratory of Specialty Fiber Optics and Advanced Communication, Shanghai University, Shanghai, 200444, China

[2] Aston Institute of Photonic Technologies (AIPT), Aston University, Birmingham, B4 7ET, United Kingdom

E-mail: *mouc1@shu.edu.cn*

†these authors contributed equally to this work

Keywords: ultrafast fiber lasers, mode locking, carbon nanotubes, polymer composites, saturable absorbers

Abstract: Carbon nanotube-polymer composite films are key elements in wide spread photonic and optoelectronic applications. One particular successful application is to produce ultrashort optical pulses in laser cavity. Nevertheless, such composite film may suffer from severe humidity/water degradation, from which the laser may even stop generating regular pulses. Here, we fabricate surfactant free carbon nanotubes (CNT)-styrene methyl-methacrylate (SMMA) polymer composite film. Based on such film-type saturable absorber (SA), a self-starting passively mode-locked erbium-doped fiber laser (EDFL) with the capability of generating ~1 ps pulses is demonstrated. On the perspective of experimental measurements and numerical simulations, we confirm the effectiveness of saturable absorber in generating ultrashort pulses. The operating composite film can survive under fully immersed water condition for ~~10~~30 days. More importantly, after the non-operating composite film has been fully soaked in the water tank for 2 days, it can still mode-lock the laser as it had been in dry air condition, confirming the humidity resistance capability. In addition, we experimentally find that the mechanical packaging of composite film has an impact on the survival time of composite film under water immersion.

1. Introduction

Ultrafast pulse generated by compact mode-locked fiber laser is currently essential for various applications such as material processing, optical frequency comb, remote sensing, and biological imaging, *etc*.[1] Accurate nano-manipulation of materials, long distance low bit error rate communication, ideal optical clock source, reliable optical frequency comb and precise laser surgery all emphasize the stability of mode-locked pulses, an important index of output pulses quality. Noise fluctuation, polarization disturbance, temperature drift and mechanical vibration probably account for the time-domain amplitude instability, time jitter noise, phase noise or pulses interval irregularity of mode locking, and even cause mode-locking lost in serious cases. Stimulated by the rapid expansion of laser technology and the increasing demand for underwater operation, potential applications in marine or atmospheric environments (*e.g.*, communication, imaging and sensing, *etc*.)[2] broaden the development prospect of environmentally stable ultrafast laser sources. Thus, researchers have been endeavoring to improve the steady output of ultrafast lasers against diverse conditions and perturbations. Nevertheless, most previous investigations have been focusing on the influence of polarization sensitivity, pressure, strain and temperature change in the surrounding environments on system robustness. Despite the reliable performance of photonic devices such as SA at stable laboratory conditions, extreme environmental factors such as humidity and moisture are the most challenging concern of promoting CNT SA into practical industrial application. On the other hand, the on-growing market for ultrafast lasers in various industrial sectors eagers for low cost & compact sources at harsh environment, *i. e*. high humidity, high temperature.

The realization of ultrashort pulses ordinarily relies on an essential element ~~saturable absorber (SA)~~ SA to facilitate ultrashort pulses generation. By far, the most commercially favored SA is semiconductor saturable absorption mirrors (SESAMs) with advantages of mature fabrication process.[3] However, its expensive preparation procedure, narrow operation bandwidth, poor compatibility with fibers and high demand for long-term environmental stability is challenging. Nano-materials based SAs have come into prominence for decades due to the outstanding third-order nonlinear effect, remarkable fast loss modulation, wide operation wavelength response.[4] As the emerging materials, two-dimensional nano-materials[5] such as graphene, topological insulators, transition metal dichalcogenides, black phosphorus, *etc*. have broadened our horizons into novel nonlinear optical materials.[6] Despites their extraordinary nonlinear optical properties, lacking the foundation of industrialization leads to specifically designed nano-sized two-dimensional materials difficult in large scale low-cost production.

~~Carbon nanotubes (CNTs)~~ CNTs have promoted the rapid advance of optoelectronics and photonics since its high third order susceptibility $\chi^{(3)}$ (magnitude about 10^{-8} esu)[7] being uncovered. Besides intrinsic advantages of wideband optical absorption spectrum (UV to near IR), fast carrier recovery time (< 1 ps) and low saturable influence,[8] the mature processing and fabrication techniques render single wall CNTs (SWCNTs) to be competitive SAs. The earliest proposed CNT SA to produce mode locked pulses is demonstrated by Set *et.al*.[9] After that, numerous implementation approaches have been attempted to efficient exploitation of CNT to fit different requirements.[9b, 10]

Among them, incorporation of SWCNTs into polymer[11] is mostly desirable benefiting from ease and low-cost manufacture, reproducibility and controllability, robust mechanical support and protection from exposure to air degradation. Embedding individual carbon nanotubes uniformly in matrix facilitates a fine control over the distribution of SWCNTs in order to avoid detrimental effects arising from agglomerating and bundling.[12] Ease of polymer processing would take advantages of flexible and diverse fabrication controllability. Additionally, the polymer matrix can offer precise manipulation of the nonlinearity parameter (recovery time, saturation intensity, non-saturable loss and modulation depth) of SA by engineering the film thickness, bundle size, nanotubes concentration and diameter distribution.

From a practical point of view, there is a strong need for a long-term reliable SA with excellent water resistance since flexible and portable SAs are being employed in more diverse environmental conditions. Therefore, features of host polymer are obliged to be carefully deliberate to better retain the nonlinear properties of CNTs in practical application: (1) The moisture induced hygroscopic swelling in the polymer will lead to the change of internal stress in the polymer substrate,[13] followed by the detrimental effect on stable mode locking. (2) Furthermore, polymers based matrices also suffer from thermally instability under high pump power induced strong heat damage.[14] (3) In addition, polymers usually require to minimize vibration overtones losses[15] in the operation range, contributing less to unsaturated loss. (4) Other conditions such as mechanically robustness, chemical stability and even manufacture complexity are worth to evaluate repeatedly. Host polymers readily used for optical applications include polymethylmethacrylate (PMMA)[16], polycarbonate (PC)[17], polyvinyl alcohol (PVA)[18], carboxymethyl cellulose (CMC)[19], polyimides (PI)[20], polyethylene terephthalate (PET)[21] . As a widely used water-soluble host polymer, PVA has excellent film-forming and smooth morphology beneficial to the film formation[22] as well as high oxygen and aromatic barrier to the distortion of outside environment. However, PVA exhibits a tendency to lose its transparency in air, due to the presence of O-H groups promoting the water molecules' *

absorption (from 1300 to 1700 nm).[15] Due to the lack of mechanical flexible component groups, PMMA[23] and PC[24] suffer from the disadvantage of brittleness. Upon exposure to prolonged harsh laser irradiation damage, low glass-transition temperature cannot be tolerated in polymers matrices such as PET, PVA, PMMA. *etc*. Sealing the CNTs in inertial gas can be effective solutions for external degradation,[25] but limited by the complex system for real applications, such as humid weather and marine environment.[2b, 26] Simultaneously, it destroys the structure integration of SA device.

Styrene methyl-methacrylate (SMMA)[13] is an ideal host polymer to fabricate moisture resistant composite film. SMMA exhibits clear advantages such as (1) broadband high optical transparency which facilitates the reduction of non-saturable loss; (2) relative low moisture absorption which capable of operating in adverse humidity environment; (3) high glass transition temperature (T_g > 120 °C) against the heat sensitivity; (4) mechanically flexibility contributes from styrene component groups; (5) high solvent compatibility to *N*-Methyl-2-pyrollidone (NMP) , an ideal carbon nanotube solvent because its surface energy matches with carbon nanotubes surface to overcome van der Waals interaction.[11, 27] The insoluble unfunctionalized CNTs impose restrictions on dispersion treatment of CNTs in majority organic and inorganic solvents. Concurrently, the enthalpy of mixing pure NMP with carbon nanotubes is approximately zero due to the interaction, so the free energy of mixing is negative in favor of dispersing CNTs.[28]

Here, we disperse SWCNTs into NMP directly and fabricate SWCNT-SMMA film with high moisture endurance. The as-fabricated film exhibits clear nonlinear optical absorption. To obtain conventional soliton mode-locked single-pulse, we construct a ring all-fiber Er-doped ultrafast fiber laser and apply SWCNT-SMMA film for mode locking. Stable mode-locking for more than 720 hours have been demonstrated. Furthermore, we experimentally prove that pristine SWCNT-SMMA film can still be used as a SA after soaking in water for 48 hours, and the mode locking state remains almost unchanged when compared to the laser using SWCNT-SMMA film without water immersion. In addition, we found that the stability of the mode-locking state of the fully water-immersed saturable absorber largely depends on the packaging of the fiber connector.

2. Results and Discussion

2.1. SWCNT Dispersion Characterization

A solution-based tip ultrasonication process is conducted on SWCNT powders in NMP to obtain certain loading of CNT dispersion, which is described in the *Experimental Section* in detail. **Figure 1a** describes the transmission electron microscope (TEM) image of the filtered

SWCNT dispersion in NMP. Two individual SWCNTs of diameter less than 2 nm can be clearly identified. The inset of **Figure 1a** describes the photograph of SWCNT dispersion. UV-VIS-NIR spectrophotometer is utilized to measure the linear optical absorption of CNT dispersion within 400~1600 nm wavelength. The input probe light excites particular resonant tubes with diameter distribution coincides with allowed specific gap energy transitions, which in turn enhance absorption peaks at given wavelength. The absorption spectrum in **Figure 1b** shows pronounced peak absorption bands from 1100 to 1600 nm covering the entire Er-doped fiber gain bandwidth. These peaks are decided by the mean diameter of semiconductor CNTs (0.8 ~ 1.2 nm), and the broad band shoulders are due to the presence of bundles. Discrete feature coincides well with allowed E_{11} transition between first van Hove singularities. The secondary peaks at 600~900 nm are recognized as typical E_{22} energy transition of semiconductor CNTs.[29] To estimate the approximate concentration of as-filtered SWCNTs in NMP, we calculate it according to the following Beer-Lambert law $A_\lambda = \alpha_\lambda\, l\, c$, where A_λ denotes the absorption value at certificate wavelength λ, l is the optical path length, c is the unknown concentration and α_λ indicates the extinction coefficient at wavelength λ. The formula shows that concentration of dispersion scales approximately linearly with absorbance per unit optical path. Owing to the well-matched absorption peak at 506 nm and 660 nm in **Figure 1b** with previous report,[28] we utilize α_{506} = 4820 L g^{-1} m^{-1} and α_{660} = 4200 L g^{-1} m^{-1} to assess the final concentration. The resultant concentration is ~0.01 mg mL^{-1}, indicating reliable dispersion efficiency compared to the demonstrated dispersion limit of ~0.02 mg mL^{-1}.[30] To further achieve the desired higher loading to SWCNTs, the preparation procedure can be optimized by adding dispersion molecules such as surfactants which permit better interaction between nanotubes and solvents.[31] It is known that simple utilization of a linear polymer poly(vinylpyrrolidone) (PVP) as dispersant assists in achieving spontaneously 'de-bundled' stable CNT dispersions in NMP.[32] Although such scheme promotes the amount of CNTs loading (over one order of magnitude) in pristine NMP and thermodynamic stability ascribe to suppressing the re-aggregation of CNTs, the existence of hydrophilic polar groups induces humidity sensitivity, due to moisture absorption and swelling of PVP in high humidity which is considered an obstacle in humidity resistant application.

2.2. SWCNT-SMMA Composite Characterization

Here, we simply fabricate SWCNT-SMMA composite based on solution-blending method, which ensures the processability and compatibility of photonic components. The complete procedure of fabrication is demonstrated in *Experimental Section*. **Figure 1c** illustrates the micro morphology of the composite surface characterized by scanning electron microscope

(SEM). The SWCNTs are well dispersed and uniformly distributed into the SMMA polymer, thus no large aggregations can be observed from the SEM image. Moreover, moderate characteristic structure proves that the composite surface is very uniform. The attained ~50 μm thick semi-transparent film is shown in inset of **Figure 1c**.

Observations on optical absorption of composite film are made by UV-VIS-NIR spectrophotometer as demonstrated in **Figure 1d**. The absorption of pure SMMA film reveals the polymer with high broadband transparency has negligible effect on the absorption of film. Although it has a strong absorbance peak at ~1680 nm, it does not have a notable impact on our operation range. Distinct absorption peaks located at 1179 nm and 1322 nm in composite film can be well identified. Moreover, 20 meV red-shift of mentioned absorption peaks in composite state compared to dispersion state indicates that, dielectric constant of electron polarization increases attributed to dielectric environment variations.[33] As bundled SWCNTs in composite contribute to the decrease of optical transition emission, consequently discernible peaks shifting appear. Simultaneously, mechanical internal stress changes caused by polymer encirclement would also lead to dielectric screening effect.[34]

The morphology and degree of uniformity of polymer composites are also studied by optical microscope. Optical micrograph of film surface from top view is shown in inset of **Figure 1d**. We deliberately focus on the edge of the film to clearly show the film's featureless surface. The obtained SWCNT-SMMA film hardly exists prominent micro-meter scale aggregations and agglomerations, as well as visible bubbles, cracks, impurities, and other visual physical defects. Its weak contribution to unsaturated loss is demonstrated by the excellent optical transparency and uniformity.

The Raman spectra are obtained by 633 nm excitation wavelengths light source as depicted by **Figure 1e**. One of the characteristic modes of CNTs are the radial-breathing modes (RBM) that demonstrate in-plane expansion and contraction vibration of carbon atoms in the radial direction. The frequency of RBM is inversely proportional to the diameter of carbon nanotubes. The most intense RBM around 257 cm^{-1} range can be observed in **Figure 1e**. Based on the empirical formula $\omega_{RBM}=\frac{A}{d_t}+B$, with A = 234 nm·cm^{-1} and B =10 cm^{-1}, we can estimate the distribution of d_t is 0.94 nm, correlates well with the 1.5 μm absorption band (photo energy of ~0.8 eV)[35]. The existence of prominent G modes in the 1500~1600 cm^{-1} range derives from double degenerate phonon modes of the hexagonal sp^2 bonding lattices. Due to the E_{2g} phonon splitting in graphene structure, G modes usually consist of two asymmetric feature peaks. The low-wave number component G^- mode (~1550 cm^{-1}) comes from adjacent carbon atoms vibration in the circumferential direction, and the high wave number component G^+ mode

(~1590 cm^{-1}) is related to the vibration of atoms along tube axis direction. The *D* modes in the 1250~1350 cm^{-1} range stem from the sp^3 hybridize vibration mode associated with the disordered graphene edge. A relatively low *D* peak confirms that the film is pure and contains relatively less defects. Generally, the defect degree of carbon nanotubes can be characterized by the intensity ratio of *D* and *G* modes. The small value of ~~0.24~~0.1 from our measurement indicates that the composite introduces negligible defect to carbon nanotube structure, and preserving the outstanding electronic properties. The *2D* peak (around 2600 cm^{-1}) represents the overtone of the *D* modes, with regard to a defect-induced second-order two phonon process.[36]

Saturable absorption is a nonlinear process where the optical absorption decreases with the increasing probe peak intensity. The saturable absorption curves shown in **Figure 1f** is obtained by power dependent transmittance measurement. The setup is described elaborately in the *Experimental Section*. As we increase the input optical intensity from 0.3 to 97 MW cm^{-2}, we record the optical transmission of the SA film. It can be seen that the nonlinear transmission of CNTs increases with the incident optical intensity and saturates at certain value. We fit the achieved power dependent transmittance according to the formula[37],

$$T(I) = 1 - \Delta T \cdot exp\left(-\frac{I}{I_{sat}}\right) - T_{ns} \quad \textbf{(1)}$$

where $T(I)$ stands for the power dependent transmission, I defines the incident intensity, ΔT represents the modulation depth of 3.5%, T_{ns} denotes non-saturable loss of 58% and I_{sat} indicates saturation peak intensity of 7.53 MW cm^{-2}, respectively. The modulation depth is not particularly high due to the loading limit of CNTs in the composites. A larger modulation depth SA should be more effective for stabilizing the single-pulse operation as well as for better self-starting. However, it is advantageous that the non-saturable loss is moderate thus scattering from residual bundles, amorphous carbon and impurities can be suppressed. Trade-offs must be made for the desired optimal parameters of SWCNT film. I_{sat} of 7.53 $MWcm^{-2}$ implies only little energy is sufficient for SA to initiate stable mode-locking.

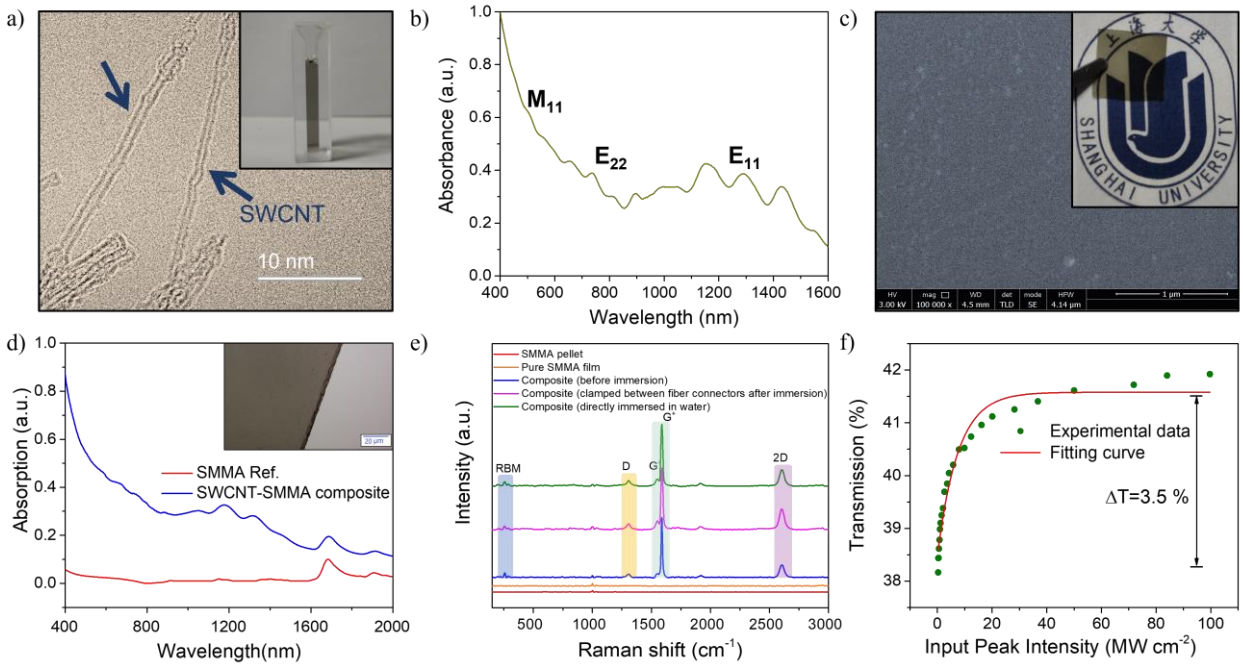

Figure 1. a) TEM micrograph of the SWCNT dispersed in NMP on the scale of 10 nm. Inset: Photograph of SWCNT dispersion. b) Absorption spectrum of SWCNT dispersion. c) SEM micrograph of SWCNT-SMMA composite surface on the scale of 1 μm. Inset: Photograph of SWCNT-SMMA film. d) Absorption spectrum of SWCNT-SMMA composite Inset: Optical micrograph of SWCNT-SMMA film. (top view) e) Raman spectra of source SMMA pellet (red), pure SMMA film (orange), SWCNT-SMMA composite before water immersion (blue), SWCNT-SMMA composite clamped between ferrule connectors after water immersion (purple), pristine SWCNT-SMMA film under water immersion for 2 days (green). f) Measured nonlinear optical transmission of SWCNT-SMMA SA as a function of input peak intensity.

2.3. Experiment and Simulation of SWCNT-SMMA Mode-Locked Fiber Laser Pulse Generation

To verify the feasibility and stability of the SWCNT-SMMA SA, we design a mode-locked Er-doped fiber laser as illustrated in **Figure 2**. The total cavity length is approximately ~7.67 m, consisting of ~1m of highly doped Erbium fiber (EDF, Liekki Er80 - 8/125), with a negative group velocity dispersion (GVD) of -20 ps^2 km^{-1} as active gain medium. Consisting of single mode fiber (SMF) with GVD of -22.8 ps^2 km^{-1}, the managed net cavity dispersion is -0.174 ps^2, consequently the laser is expected to operate in anomalous regime thus facilitates the generation of conventional solitons (CS). The EDF is pumped by a 980 nm laser diode (LD) via a 980/1550 wavelength division multiplexer (WDM) coupler. The circulating pulse is extracted 30% for analysis with the assistant of 70:30 output coupler (OC). We cut the film in 2 * 2 mm^2 size and

sandwich the piece between two fiber ends through a ferrule connector to assemble the SA. **Figure 2** shows a photograph of SWCNT-SMMA SA-incorporated fiber patch cord. A polarization independent isolator (PI-ISO) is subsequently inserted into the cavity to prevent deleterious back reflection and ensure single direction propagation. Polarization controller (PC) is utilized for adjusting the optimal intracavity polarization state and intra-cavity birefringence.

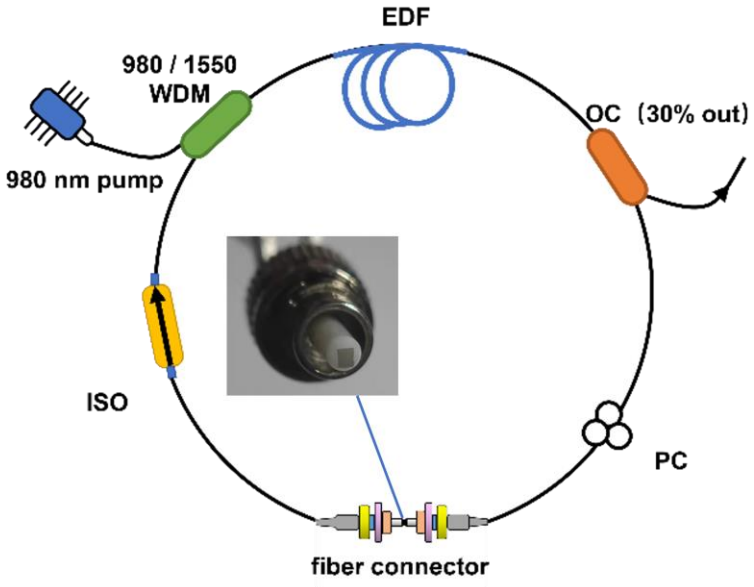

Figure 2. Experimental setup of SWCNT-SMMA SA based passively mode-locked erbium-doped fiber laser.

We observe continuous wave (CW) operation settles at 1565 nm under the pump power level of 50 mW. When the pump power is increased to 78.5 mW, self-starting mode-locked pulses can be initiated without the necessity of tuning intracavity polarization state. This proves the demonstrated composite film is polarization independent. Due to the interaction between anomalous cavity dispersion and nonlinear Kerr effect, it is expected that conventional solitons emerge. A pulse of central wavelength of 1564.65 nm and a 3-dB spectral bandwidth of 2.75 nm can be obtained, as shown in **Figure 3a**. **Figure 3b** depicts the pulse trains with an interval of 36.96 ns, corresponding to the fundamental repetition rates of 27.06 MHz. **Figure 3c** measures the radio frequency signals centered at 27.06 MHz in 1 MHz span, from which the fundamental frequency signal to noise ratio (SNR) reaches 60 dB, manifesting the outstanding quality of propagating pulses. The inset in **Figure 3c** shows the RF signals in 3 GHz span. The flat spectrum indicates the stability of fiber laser. **Figure 3d** is a second harmonic generation (SHG) autocorrelation trace (AC) of the mode-locked pulses with FWHM of 1.601 ps. Assuming a $sech^2$ temporal profile, the deconvolution gives a pulse duration of 1.038 ps. The calculated time bandwidth product (TBP) is 0.35, exhibiting almost transform-limited pulse

output. In the meantime, the output power is measured to be ~0.9 mW, corresponding to the single-pulse energy of ~33.48 pJ.

The optical spectral sidebands are fingerprints of CS. To adjust the periodic interferences in fiber laser, solitons shade a portion of their energy in the form of radiative waves, and stimulate discrete Kelly sidebands appearing on both sides of the central wavelength. The positions of Kelly sidebands on the spectrum are determined by the cavity dispersion and nonlinearity. On the premise of phase matching, the wavelength separation with the central wavelength $\Delta\lambda_m$ can be calculated by

$$\Delta\lambda_{\mathrm{m}} = \pm\frac{{\lambda_0}^2}{2\pi c\tau_0}\sqrt{\frac{4\pi{\tau_0}^2}{Z_a|\beta_2|}\mathrm{m}-1} \quad \textbf{(2)}$$

where λ stands for the center wavelength of 1564.65 nm, τ_0 describes a pulse duration of 1.038 ps, integer m defines the order of sidebands, Z_a is the cavity length and β_2 represents the group velocity dispersion. Assuming m equals 1, the calculated first-order sidebands separations with central wavelength $\Delta\lambda$ is 10.97 nm. The results agree well with actual Kelly sidebands distributions at 1575.89 nm and 1553.64 nm respectively shown in **Figure 3a**.

Further increasing pump power leads to the variation of the gain-and-loss distribution, which makes the peak of the optical spectrum shift to another wavelength. For each pump power, the pulse bandwidth and pulse duration can be optimized and fine-tuned by adjusting the PC orientation. Nevertheless, the laser maintains mode-locking during the adjustment. We take out the SA from cavity and no mode locking could be obtained again with any manipulation, which proves that the mode locking is merely governed by our thin film.

No visible optical damage of SA device can be observed even up to our maximum available pump power of 660 mW. The speculated critical damage threshold is higher than ~20 mW, with regard to high glass transition temperature of SMMA, which serves as a sign of heat repellence. Higher T_g of host material endows SA with desirable thermal ruggedness and robustness.

In order to acquire better understanding of the SWCNT-SMMA SA effect on mode locking, we conduct numerical analysis of the conventional soliton behavior inside the cavity. The soliton solution is processed based on extended nonlinear Schrödinger equation with comprehensive considering the impact of gain saturation, cavity loss, output coupling, second anomalous group-velocity dispersion, self-phase modulation, saturable absorption and other factors with regard to the oscillating pulses. Most of the parameters used in the simulation are obtained by referring to the actual measurement, such as the parameters of SA, EDF and SMF. Parameters not actually confirmed, such as the recovery time of SA, nonlinear parameters of

SMF and EDF, shall be corrected according to the experimental conditions. A standard split-step Fourier algorithm is utilized to solve the equation. Random quantum noise is assumed as initial signal field. Several numbers of loops propagation in cavity give rise to the convergence of electric field envelope. Ultimate steady conventional soliton pulses can be obtained with optical spectrum and AC trace shown in **Figure 3e** and **Figure 3f**, respectively. The outcome reveals the pulse with 3-dB bandwidth of 2.75 nm and temporal pulse width of 935 fs. The slight pulse width broaden can be explained that a section of SMF spliced to the output coupler trigger a small amplitude broadening of the transform-limited pulse width. Simulations exhibit well agreement with experimental results.

It is worth mentioning that the mode-locking performance will be affected by the fabrication procedure. Owing to our surfactant free fabrication process, it is difficult to further increase the loading of SWCNTs without surface functionalization in organic solvent NMP. Although the concentration of SWCNTs in composite is lower compared to the surfactant-aided *(e.g.* PVP) composite, it indirectly affects the modulation depth of SA, and deteriorates self-starting threshold and pulse width narrowing. On the contrary, low loading prevents from large agglomeration of SWCNTs, in favor of decreasing the SA unsaturable loss. As a result, it is beneficial to improve the laser efficiency and depress the insertion loss.

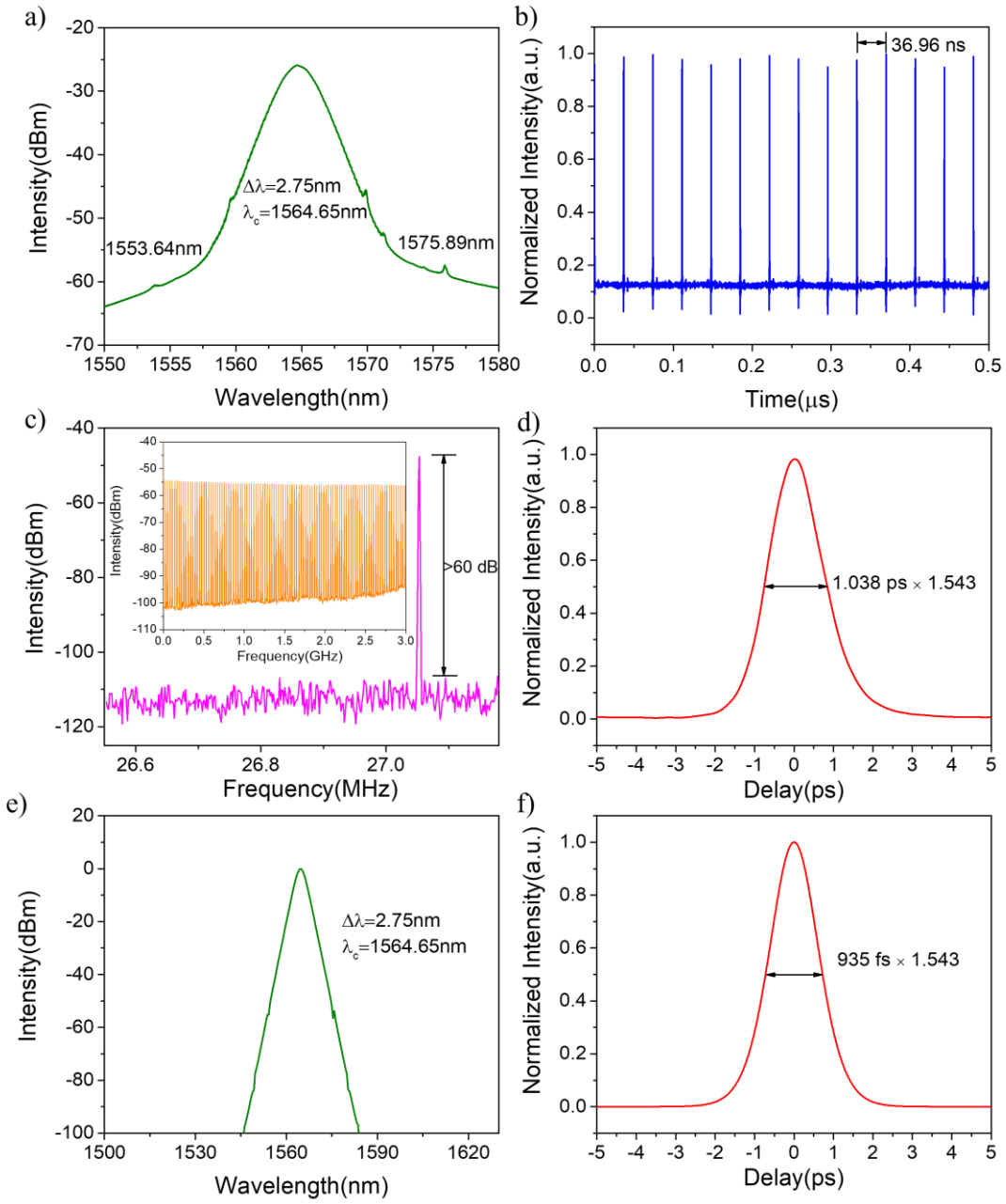

Figure 3. a-d) Typical output performances of ultrafast lasers mode-locked by SWCNT-SMMA SA under pump power of 78.5 mW. a) Optical spectrum with resolution of 0.02 nm. b) The oscilloscope trace in time domain. c) RF spectra at 27.06 MHz. Inset: RF spectra within 3 GHz span. d) AC trace of the pulse delivered from cavity directly. e-f) Simulated results of single pulse CSs. e) Optical spectrum. f) AC profile.

2.4. Humidity Stability of SWCNT-SMMA Film

For the verification of the hydrophobicity of the composite film SA, we initially started by a method similar to previous study[13]. The cavity is placed in a stable laboratory environment

condition with low thermal variations and minimal mechanical disturbance. The sensitivity of small temperature drift and vibration is not noticed during the experiment.

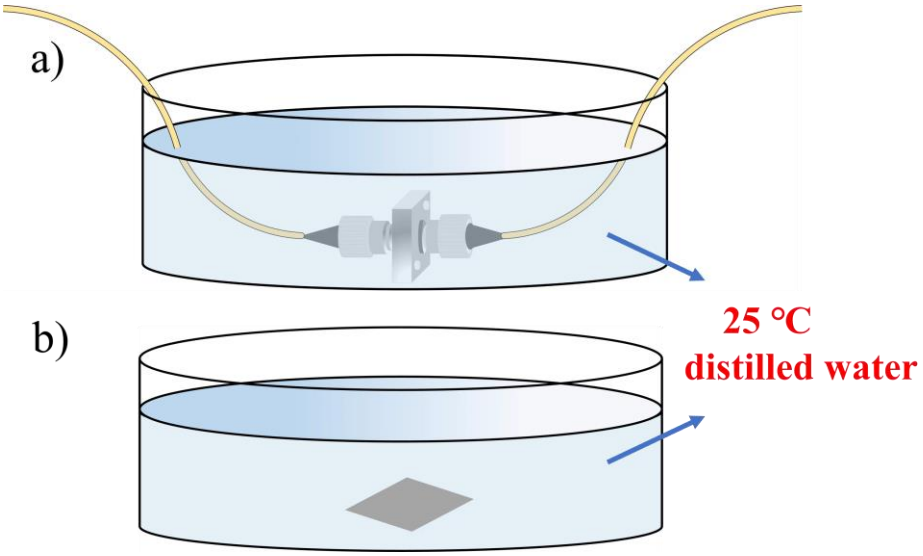

Figure 4. Schematic diagram of a) Humidity stability experiment of SA clamped between ferrule connectors. b) Direct water immersion experiment of composite film.

Though SWCNT-SMMA SA clamped between fiber connectors cannot be observed directly, we can analyze the operation stability under harsh water immersion through optical spectrum profile. Fiber-ferrule-embedded SMMA SA is directly immersed in 25 °C water as **Figure 4a** demonstrated. Stability test is ascertained by the long-term operating continuously for ~~240~~ 720 hours (~~10~~ 30 days) monitoring without losing mode-locking as shown in **Figure 5a**. The optical spectra of pulses remain relatively stable without obvious differences as **Figure 5b** depicts. Although the mode locking state of SMMA SA has slightly deteriorated during the experiment, we speculate that it is not caused by the water absorption of the film, but the water entering the ferrule connector contacts with the film surface, which directly affects the stability of mode locking. The thermal effect and the oxidation of film are also possible candidates to cause the subtle property change of the clamped film as well. ~~In order to check this conjecture, we wipe out the water on the surface of the unlocked SA and put it back into the same laser setup. The results exhibit that it can still mode lock even without changing the original operation state.~~ We measure the immersed SA by Raman spectroscopy and similar spectrum profile proves that its quality has not been changed as shown in **Figure 1e**. This is a strong-evidence that it can tolerate humidity.

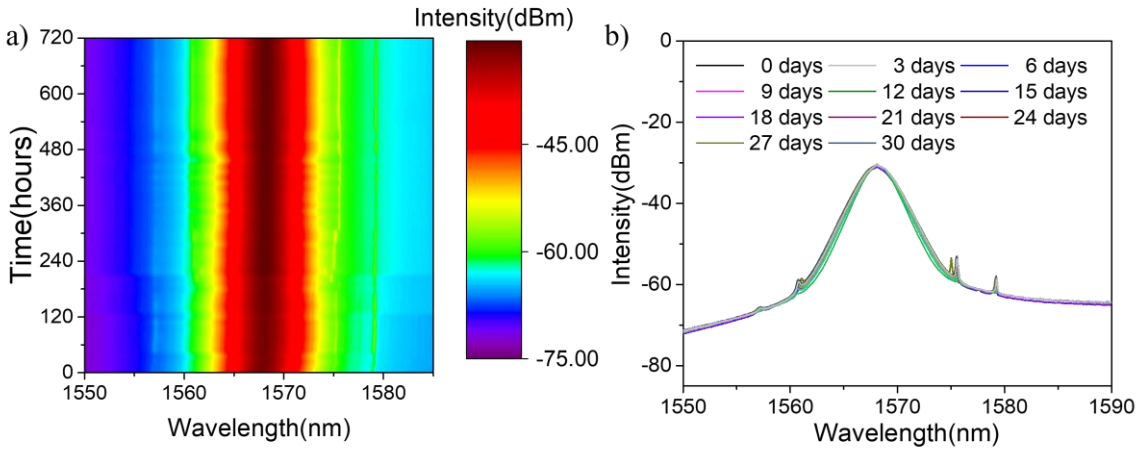

Figure 5. Optical spectra as a function of time for SWCNT-SMMA SA under water immersion. a) Long-term stability under water immersion across ~~240~~ 720 h. b) The shift of optical spectra across ~~240~~ 720 h.

To straightly assess the SWCNT-SMMA composites' capability of withstanding water erosion, we also immerse the SWCNT-SMMA composite film directly in water, as **Figure 4b** illustrates. The composite film can still mode-lock normally after 2 days soaked with no obvious variations in Raman spectra illustrated in **Figure 1e**. The similar optical spectra traces in dry air and after water immersion for 2 days shown in **Figure 6a** confirm the superb water-resistant performance of SWCNT-SMMA film. Almost overlapped AC traces depicted in **Figure 6b** also manifest that the film is inherent water resistant. Thus, it is verified that the SMMA film composed of hydrophobic components will not be significantly affected by moisture, humidity and even water. In order to ensure that our complete immersion scheme creates harsh humidity environment and intuitively highlight the water resistance of SMMA, we choose the classic water-soluble polymer PVA based SA (the preparation of PVA SA could refer [38]) for comparison. Under the same circumstances in **Figure 4b**, the PVA SA dissolves slowly after immersion in water for 10 minutes, suggesting the intrinsic humidity instability of PVA. Naturally, it does not possess the stability of working in humidity environment for long time. Similarly, it also manifests that this extreme water environment has a significant impact on the composite film, in which the SMMA and PVA composite films exhibit remarkable different behavior, respectively.

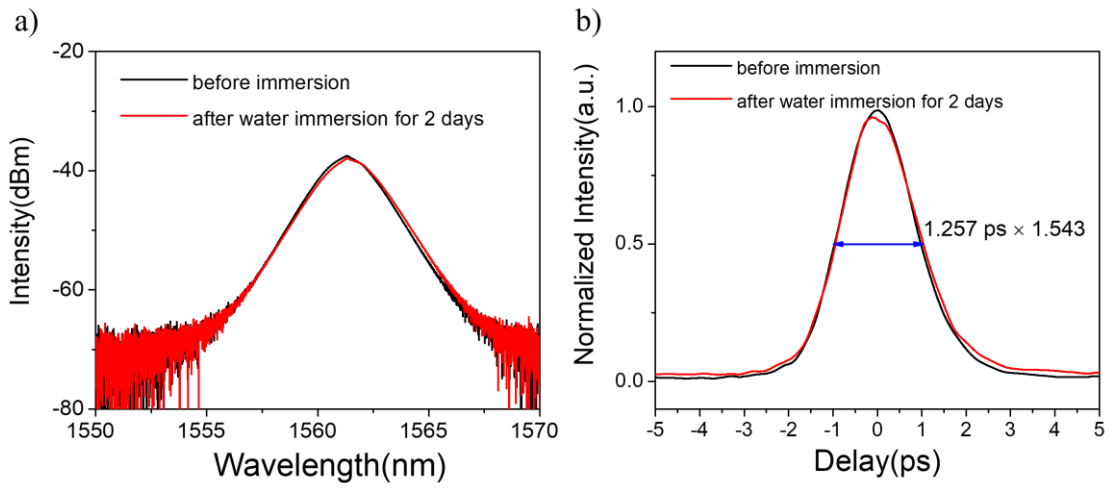

Figure 6. a) Optical spectra of SWCNT-SMMA film before immersion (red), after water immersion for 2 days (black). b) AC traces of the pulse from SWCNT-SMMA SA.

Furthermore, we also noticed that the mechanical packaging of fiber ferrule has a non-negligible influence in the experiment. For comparison, we place two PVA SAs on the fiber ends and embed them with fiber connectors, respectively ~~(the preparation of PVA SA could refer [38])~~. We intentionally make the degree of mechanical tightness between fiber connectors remarkable different in the two sets of tests (Set A relatively looser, Set B relatively tighter), while ensure other conditions are the same. The packaged PVA SAs are then immersed in room-temperature water (approximately 25 °C) as seen from **Figure 4a**, indicating a harsh humidity environment. We fix pump power at stable mode locking state and carry out repeated scans at 1h intervals. The results are plotted in **Figure 7**. In set A, the monitoring is carried out for 5 hours as shown in **Figure 7a**. Significant wavelength drift is observed for the first several hours, and the mode-locked pulse switches to CW within 5 hours monitoring. In set B depicted in **Figure 7b** (200 hours monitoring), subtle changes emerge in the first few hours with Kelly sidebands deviations and the central wavelength shifts. In the subsequent period, excellent packaged PVA SA operates continuously long-term without losing mode-locking although some distinct fluctuations can be seen in the optical spectrum. It maintains mode locking for quite a long time but finally switches to CW after 204 hours operation. After losing mode locking, no residue PVA film on fiber patch cord can be found, indicating the PVA polymer has been completely dissolved.

Our experimental observation clearly shows that different packages result in the different speed of water penetration into fiber ferrules. Hence, we can conclude that packaging is another key factor affecting the mode locking stability in a humid environment. Therefore, it

is lack of rigorous to prove that SA can stably work in humidity environment only by completely immersing fiber connector in water[39].

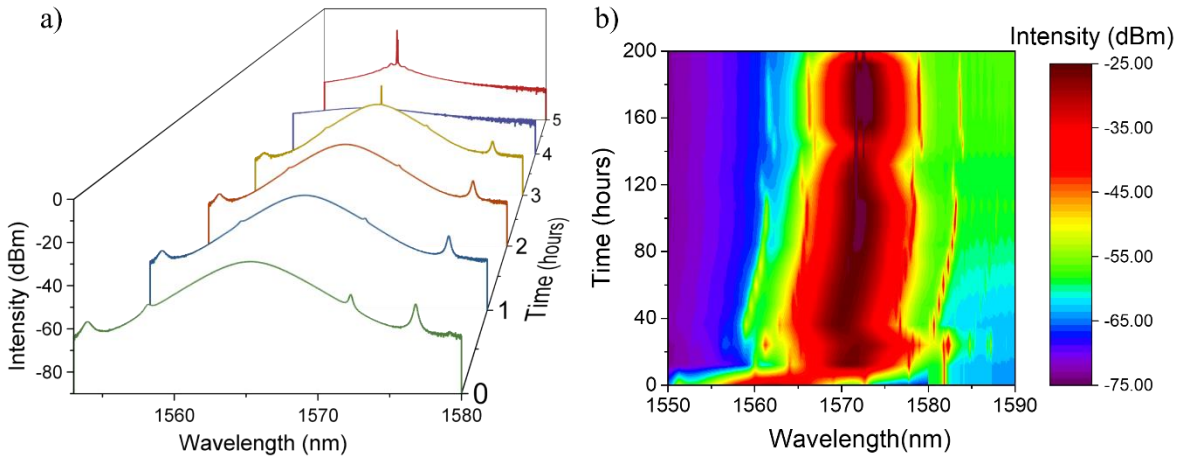

Figure 7. Optical spectra as a function of time for two SWCNT-PVA SAs under water immersion. a) Set A across 5 hrs. b) Set B across 200 hrs.

The performance gap against humidity of these two polymers can be explained from the perspective of group composition. SMMA, as a typical linear polymer comonomers, consists of styrene and methyl-methacrylate group. Due to the existence of ester group (carbonyl group) in MMA monomers, it has negligible hygroscopicity through hydrogen bonding. However, the presence of highly non-polar styrene groups provides hydrophobic aromatic ring structure. Moreover, CNTs are insoluble in water. So external water incursion is mitigated for inherent hydrophobic nature of composites. Despite small dimension swelling is difficult to inhibit, SWCNT-SMMA SA largely preserves its properties against the penetration of water, so as to achieve excellent long-term steady operation. Conversely, the hydrophilic carbonyl groups of PVA attract water molecules through the formation of hydrogen bonds. As a result, PVA based SA suffers from premature failures. In the ferrule connectors, moisture permeation is a gradual and persistent process, leading to hygroscopic swelling of polymeric film with affinity for moisture. Subsequently, PVA based sample would undergo the breaking of chemical bonds and composition. Sustained water erosion would completely dissolve the hydrophilic polymer.

3. Conclusions and Outlooks

At present, the proposed SA commonly performs well in laboratory environment. Nevertheless, most practical applications face a severe issue, that is, the diverse climate, humid condition and other environmental factors have put forward some requirements for the material-based SA. For this purpose, hydrophobic polymeric embedding is essential with huge advantages of

inherent water resistance property. In summary, we provide in-sights into current challenges of host polymer based saturable absorber and report a highly stable humidity resistant SA with ability to operate even in aqueous environments. In addition, we characterize its performance as a wonderful SA. Moreover, we demonstrate a passively mode-locked erbium-doped fiber laser based on the SWCNT-SMMA SA. Further experimental results and theoretical simulations of the propagating single pulse output performance are presented and the numerical simulations confirm the experimental observations very well. The humidity stability is discussed and investigated. Consequently, we confirm that SWCNT-SMMA SA is an excellent candidate material SA for practical device applications against humidity. Moreover, as SWCNT would be able to work for broadband photonic application through proper distribution of tube diameters, *etc*, it can be envisioned that the demonstrated method may extend into other operation wavelength such as mid-infrared. Future efforts shall allow controlling the characteristics of the polymers by modification so as to further extend its environmentally stability against more complex and changeable extreme situations. We believe that our results are of great significance for further promote research interests and advanced insights into nonlinear photonic device under harsh environment.

4. Experimental Section

SWCNT Dispersion Preparation: We select commercial-available SWCNTs synthesized by HiPco (purity > 85%, Nano Integris) as source material. Its mean diameter is 0.8 ~ 1.2 nm corresponding to absorption band from 1300 nm to 1600 nm. Several grams of SWCNT are mixed with 10 mL NMP at an initial concentration of 0.3 mg mL^{-1}. The CNT powders are ultrasonicated (Bioruptor, Diagenode) for 4 hours. The 70% supernatant of dispersions is immediately vacuum filtered by binder free glass fiber filter (Whatman, 0.7 µm pore size retention) to remove the residual large bundles, catalyst, sedimentations and amorphous carbon.

SWCNT-SMMA Composite Fabrication: 100 mg SMMA pellets (~~cat no.~~CAS 25034-86-0, average Mw 100,000~150,000, Sigma-Aldrich) as host matrix is dissolved in 3 mL volume of the as-prepared CNT dispersion. The mixture is mechanically agitated by magnetic stirrers until pellets are thoroughly dissolved and uniformly distributed. Then they are poured in a glass petri dish followed by a vacuum chamber at 80 °C for 36 hours. Finally, we attain a ~50 µm thick semi-transparent film.

Characterization of Sample: TEM (JEOL, JEM 2100F) is conducted to study the nano-scale structure of the filtered SWCNT dispersion in NMP. UV–VIS–NIR absorbances of composite and dispersion are revealed by UV-VIS-NIR spectrophotometer (Hitachi Ltd,

UH4150). SEM (FEI, Nova Nano SEM, 3 kV acceleration voltage) is used to characterize the morphology of composite surface. The Raman spectra are performed by Raman spectrometer (Horiba, LabRAM HR Evolution) with the laser excited at 633 nm under ambient conditions, with the scattered light collected by 50× objective lens and the laser power to be 1 mW with the focused beam size of 1 μm.

Power Dependent Transmittance Measurement Setup: In a typical balanced twin detector system, a home-made femtosecond mode locked fiber laser is chosen as the probe light source. The home-made fiber laser working at 1566 nm provides 582 fs pulses with a repetition rate of 27 MHz, followed by an optical polarization independent isolator to avoid undesirable back reflection. A mechanical variable optical attenuator is positioned after the isolator to control the power of the probe. The power launched in both arms is measured via a commercial optical power meter (Thorlabs, PM250).

Fiber Laser Mode Locked Pulses Output Measurement: The extracted output signal light is characterized by an optical spectrum analyzer (OSA, Yokogawa AQ6370D) with a resolution bandwidth accuracy of 0.02 nm is used for detecting the optical spectrum. Additionally, an 8 GHz real-time digital oscilloscope (OSC, Keysight DSO90804A) and a radio frequency (RF) spectrum analyzer (Siglent, SSA3032X) are connected to a 12.5 GHz high speed photo-detector (PD, Newport 818-BB-51F) respectively to evaluate the characteristics of the output pulse. Meanwhile, the temporal pulse profile is examined by a commercial-available autocorrelator (Femtochrome, FR-103XL). An optical power meter (Thorlabs, PM320E) and Photodiode Power Sensor (Thorlabs, S155C) is utilized to measure the average output power.

Numerical Simulations of Mode Locked Fiber Laser: The calculation is based on commercial-available software Fiberdesk to investigate evolution of pulses dynamics. Extended nonlinear Schrödinger equation is modelled as

$$i\frac{\partial A}{\partial z} = \frac{1}{2}\beta_2\frac{\partial^2 A}{\partial T^2} - \gamma|A|^2A + i\frac{g}{2} \quad \textbf{(3)}$$

where A denotes pulses electric field envelope, The variables T and z represent the pulse local time and propagation distance, respectively, β_2 refers to the group velocity-dispersion parameter, γ is the nonlinear parameter, g stands for gain coefficient. Gain saturation and gain spectrum for EDF is expressed as

$$g = \frac{g_0}{1+\frac{E}{E_{sat}}} \quad \textbf{(4)}$$

here g_0 describes the small signal gain coefficient, E represents pump-power dependent pulse energy, E_{sat} denotes gain saturation energy. The CNT SA is modelled by classic two-level fast saturable absorber model of

$$\alpha(I) = \alpha_{ns} + \alpha_0 \left(1 - \frac{1}{1+\frac{P}{P_{sat}}}\right) \quad \textbf{(5)}$$

where α_{ns}, α_0, P_{sat} are the unsaturable absorption coefficient, modulation depth and absorption saturable energy (assuming a 10.4 μm fiber core), respectively. Related parameters for each element are provided as followed: gain of 10 dB m^{-1}, gain bandwidth of 40 nm, nonlinear parameter of 0.0017 $W^{-1}m^{-1}$ for EDF and nonlinear parameter of 0.0014 $W^{-1}m^{-1}$ for SMF. Assuming recovery time of 200 fs and focusing diameter of 10.4 μm, other parameters of fast SA are given according to our actual measurement. Couplers, SMF and other components are designed according to experience operation situations.

Acknowledgements

The authors acknowledge funding from National Natural Science Foundation of China (62135007,61975107,61605107); National Key Research and Development Program of China (2020YFB1805800); Overseas Expertise Introduction Project for Discipline Innovation (D20031); Natural Science Foundation of Shanghai (20ZR1471500).

Conflict of Interest

The authors declare no conflict of interest.

Data Availability Statement

The data that support the findings of this study are available from the corresponding author upon reasonable request.

References

[1] a)M. E. Fermann, I.Hartl, *Nature Photonics* **2013**, 7, 868; b) U. Keller, *Nature* **2003**, 424, 831; c) J. S. Harris, *IEEE Journal of Selected Topics in Quantum Electronics* **2000**, 6, 1145.

[2] a)R. Min, Z. Liu, L. Pereira, C. Yang, Q. Sui, C. Marques, *Optics & Laser Technology* **2021**, 140, 107082; b)S. P. O'Connor, L. J. Mullen, B. Cochenour, *Optical Engineering* **2014**, 53, 051403; c)J. B. Snow, J. P. Flatley, D. E. Freeman, M. A. Landry, C. E. Lindstrom, J. R. Longacre, J. A. Schwartz, in *Ocean Optics XI* , Vol. 1750, San Diego, CA, United States, **1992**.

[3] U. Keller, K. J. Weingarten, *IEEE J Selected Topics in Quantum Electronics* **1996**, 2, 435.

[4] a)S. Suresh, D. Arivuoli, *Reviews on Advanced Materials Science* **2012**, 30; b)J. Tarka, J. Boguslawski, G. Sobon, I. Pasternak, A. Przewolka, W. Strupinski, J. Sotor, *IEEE Journal of Selected Topics in Quantum Electronics* **2016**, 60.

[5] B. Fu, J. Sun, G. Wang, C. Shang, Y. Ma, J. Ma, L. Xu, V. Scardaci, *Nanophotonics* **2020**, 9, 2169.

[6] a)D. Mao, X. She, B. Du, D. Yang, W. Zhang, K. Song, X. Cui, B. Jiang, T. Peng, J. Zhao, *Scientific Reports* **2016**, 6, 23583; b)K. F. Ma.k, J. Shan, *Nature Photonics* **2016**, 10, 216; c)J. Koo, J. Park, J. Lee, Y. M. Jhon, J. H. Lee, *Optics Express* **2016**, 24, 10575.

[7] Y. C. Chen, N. R. Raravikar, L. S. Schadler, P. M. Ajayan, X. C. Zhang, *Applied Physics Letters* **2002**, 81, 975.

[8] a)S. Yamashita, *Apl Photonics* **2019**, 034301; b)J. Wang, C. Yu, R. Li, H. Dong, W. J. Blau, in *Carbon Nanotubes: Synthesis, Characterization, Applications*, Vol. 397, London, United Kingdom, **2011.**

[9] a)S. Y. Set, H. Yaguchi, Y. Tanaka, M. Jablonski, *Journal of lightwave Technology* **2004**, 22, 51; b)S. Y. Set, H. Yaguchi, Y. Tanaka, M. Jablonski, *IEEE Journal of Selected Topics in Quantum Electronics* **2004**, 10, 137.

[10] Y. W. Song, K. Morimune, S. Y. Set, S. Yamashita, *Applied Physics Letters* **2007**, 32, 148; b)Y. W. Song, S. Yamashita, C. S. Goh, S. Y. Set, *Optics Letters* **2007**, 32, 148; c)A. V. Tausenev, E. D. Obraztsova, A. S. Chernov, V. I. Konov, P. G. Kruykov, A. V. Konyashchenko, E. M. Dianov, *Applied Physics Letters* **2008**, 92, 171113; d) A. Martinez, S. Uchida, Y. W. Song, T. Ishigure, S. Yamashita, *Optics Express* **2008**, 16, 11337; e)V. V. VanyuKov, K. G. Mikheev, A. G. Nasibulin, Y. Svirko, G. M. Mikheev, *Optics Letter* **2020**, 45, 5377; f)P. Xiao, K. Wu, D. Mao, J. Chen, *Optics Express* **2019**, 27, 4188.

[11] P. M. Ajayan, O. Stephan, C. Colliex, D. Trauth, *Science* **1994**, 265, 1212.

[12] H. T. Ham, Y. S. Choi, I. J. Chung, *Journal of Colloid and Interface Science* **2005**, 286, 216.

[13] F. Torrisi, D. Popa, S. Milana, Z. Jiang, T. Hasan, E. Lidorikis, A. C. Ferrari, *Advanced Optical Materials* **2016**, 4, 1088.

[14] D. Galiakhmetova, Y. Gladush, A. Mkrtchyan, F. S. Fedorov, E. M. Khabushev, D. V. Krasnikov, R. Chinnambedu-Murugesan. E. Manuylovich, V. Dvoyrinbc, A. Rozhinb, M. Rümmeli, S. Alyatkina, P. Lagoudakis, A. G. Nasibulin, *Carbon* **2021**, 184, 941.

[15] H. Ma, A. Y. Jen, L. R. Dalton, *Advanced Materials* **2002**, 14, 1339.

[16] A. Martinez, S. Uchida, Y. W. Song, T. Ishigure, S. Yamashita, *Optics Express* **2008**, 16, 11337

[17] F. Shohda, T. Shirato, M. Nakazawa, K. Komatsu, T. Kaino, *Optics Express* **2008**, 16, 21191.

[18] Y. Sakakibara, A. G. Rozhin, H. Kataura, Y. Achiba, M. Tokumoto, *Japanese Journal of Applied Physics* **2005**, 44, 1621.

[19] N. Minami, Y. Kim, K. Miyashita, S. Kazaoui, B. Nalini, *Applied Physics Letters* **2006**, 88, 093123.

[20] T. R. Schibli, K. Minoshima, H. Kataura, E. Itoga, N. Minami, S. Kazaoui, K. Miyashita, M. Tokumoto, Y. Sakakibara, *Optics Express* **2005**, 13, 8025.

[21] H. B. Zhang, W. G. Zheng, Q. Yan, Y. Yang, J. W. Wang, Z. H. Lu, G. Y. Ji, Z. Z. Yu, *Polymer* **2010**, 51, 1191.

[22] A. H. H. Al‐Masoodi, M. F. Ismail, F. Ahmad, N. Kasim, Y. Munajat, H. Ahmad, S. Wadi Harun, *Microwave and Optical Technology Letters* **2014**, 56, 1770.

[23] J. Fineberg, S. P. Gross, M. Marder, H. L. Swinney, *Physical Review B* **1992**, 45, 5146.

[24] a)A. I. Isayev, M. Modic, *Polymer Composites* **1987**, 8, 158; b) V. V. Vanyukov, K. G. Mikheev, A. G. Nasibulin, Y. Svirko, G. M. Mikheev, *Optics Letters* **2020**, 45, 5377.

[25] S. Yamashita, A. Martinez, B. Xu, *Optical Fiber Technology* **2014**, 20, 702.

[26] B. Cochenour, L. Mullen, J. Muth, in *Ocean Sensing and Monitoring IV*, Vol. 8372, Baltimore, Maryland, United States, **2012.**

[27] K. D. Ausman, R. Piner, O. Lourie, R. S. Ruoff, M. Korobov, *The Journal of Physical Chemistry B* **2000**, 104, 8911.

[28] T. Hasan, V. Scardaci, P. H. Tan, A. G. Rozhin, W. I. Milne, A. C. Ferrari, *The Journal of Physical Chemistry C* **2007**, 111, 12594.

[29] R. B. Weisman, S. M. Bachilo, *Nano Letters* **2003**, 3, 1235.

[30] S. Giordani, S. D. Bergin, V. Nicolosi, S. Lebedkin, M. M. Kappes, W. J. Blau, J. N. Coleman, *The Journal of Physical Chemistry B* **2006**, 110, 15708.

[31] W. K. Sang, T. Kim, Y. S. Kim, H. S. Choi, H. J. Lim, S. J. Yang, C. R. Park, *Carbon* **2012**, 50, 3.

[32] T. Hasan, P. H. Tan, F. Bonaccorso, A. G. Rozhin, V. Scardaci, W. I. Milne, A. C. Ferrari, *The Journal of Physical Chemistry C* **2008**, 112, 20227.

[33] A. G. Walsh, A. N. Vamivakas, Y. Yin, S. B. Cronin, M. S. ünlü, B. B. Goldberg, A. K. Swan, *Nano Letters* **2007**, 7, 1485.

[34] J. Wu, W. Walukiewicz, W. Shan, E. Bourret-Courchesne, J. W. Ager, K. M. Yu, E. E. Haller, K. Kissell, S. M. Bachilo, R. B. Welsman, R. E. Smalley, *Physical Review Letters* **2004**, 93, 017404..

[35] H. Kataura, Y. Kumazawa, Y. Maniwa, I. Umezu, S. Suzuki, Y. Ohtsuka, Y. Achiba, *Synthetic Metals* **1999**, 103, 2555..

[36] C. Thomsen, S. Reich, in *Light Scattering in Solid IX* , Vol. 108, Springer, Berlin, Heidelberg, **1970**.

[37] Y. Lü, C. Wei, H. Zhang, Z. Kang, G. Qin, Y. Liu, *Photonics Research* **2019**, 7, 14.

[38] Q. Huang, C. Zou, T. Wang, M. A. Araimi, A. Rozhin, C. Mou, *IEEE Journal of Selected Topics in Quantum Electronics* **2019**, 25, 1.

[39] a)Y. Ge, W. Huang, F. Yang, J. Liu, C. Wang, Y. Wang, J. Guo, F. Zhang, Y. Song, S. Xu, D. Fan, H. Zhang, *Nanoscale* **2019**, 11, 6828; b)X. Jin, G. Hu, M. Zhang, T. Albrow-Owen, Z. Zheng, T. Hasan, *Nanophotonics* **2020**, 9, 2445.